Rapid crustal growth and efficient crustal recycling in the early Earth: Implications for Hadean and Archean geodynamics

Juan Carlos Rosas[1] and Jun Korenaga[1,*]

[1]Department of Geology and Geophysics, Yale University, P.O. Box 208109, New Haven, CT 06520-8109, USA

Email: juan.rosas@yale.edu (Juan Carlos Rosas), jun.korenaga@yale.edu (Jun Korenaga)

Corresponding author: Jun Korenaga

Tel: (203) 432-7381; **Fax:** (203) 432-3134

Submitted to *Earth and Planetary Science Letters*, March 2018; Revised, April 2018.

Abstract. The geodynamic regime of the early Earth remains elusive, with so far proposed hypotheses ranging from stagnant lid convection to rapid plate tectonics. Available geological data are severely limited for the first two billion years of the Earth history, and this scarcity of relevant data is often compounded by the nonuniqueness of interpretation. Here we propose that the samarium-neodymium isotope evolution, which has been suggested to be consistent with stagnant lid convection in the early Earth, may be better understood as the result of rapid crustal growth and extensive crustal recycling. We delineate the permissible scenario of crustal evolution through geochemical box modeling with the Monte Carlo sampling of the model parameter space, and our results suggest that the net growth of continental crust was complete by the end of the Hadean and that the rate of crustal recycling could have been as high as $2-4\times10^{22}$ kg Gyr^{-1} at that time and has gradually decreased since then. Such crustal evolution yields a specific prediction for the present-day distribution of crustal formation ages, which is shown to be in remarkable agreement with a recent estimate based on the global compilation of zircon age data. The mode of subsolidus mantle convection after the putative magma ocean is probably plate tectonics, but its style could have been very different from that of contemporary plate tectonics, characterized by more voluminous magmatism and more destructive subduction.

Keywords: Sm-Nd isotope systems, crust-mantle differentiation, plate tectonics

1 Introduction

Reconstructing the geodynamic regime of Earth during its first two billion years is challenging due to the paucity of relevant geological data. Rocks of Archean ages are considerably less abundant than those of Proterozoic ages, and little rock has survived from the Hadean, with the mineral zircon being the primary probe for this eon. Because of the lack of decisive observational constraints, the onset of plate tectonics or, more generally, the mode of mantle convection in the early Earth remains a controversial topic (e.g., Korenaga, 2013). The operation of plate tectonics is inherently linked to the long-term CO_2 cycle, the oxygenation of the atmosphere, and the global water cycle,

via subduction and volcanic degassing (e.g., Holland, 1984; Lyons et al., 2014; Korenaga et al., 2017). As these processes exert first-order control on the evolution of surface environment, resolving the geodynamic regime of the early Earth is essential if we wish to understand the evolution of the planet as a whole.

Existing models for mantle convection in the early Earth span stagnant lid convection (e.g., O'Neill and Debaille, 2014) to rapid plate tectonics (e.g., Sleep et al., 2014). Proponents for different models employ different kinds of observations or theoretical reasoning, and given the fundamental limitation of available geological data, it is important to examine the robustness of each of these arguments. Here we focus on the samarium-neodymium (Sm-Nd) isotope evolution, which has recently been used as key supporting evidence for stagnant lid convection in the early Earth (Debaille et al., 2013; O'Neill and Debaille, 2014). Both Sm and Nd are lithophile and incompatible elements, with Nd being slightly more incompatible than Sm. The pair of these two elements is particularly attractive for tracking crust-mantle differentiation, owing to the existence of two isotope systems with vastly different decay constants: ^{147}Sm and ^{146}Sm decay into ^{143}Nd and ^{142}Nd, respectively, with the corresponding half-lives of $\sim$106 Gyr and $\sim$103 Myr. Whereas the ^{143}Nd evolution of the depleted mantle (Fig. 1a) is commonly interpreted as the result of continental crust extraction (e.g., Bennett, 2003), the ^{142}Nd evolution (Fig. 1b) has been suggested to reflect inefficient mantle mixing associated with stagnant lid convection (Debaille et al., 2013). The amplitude of μ^{142}_{Nd} anomalies is as high as $\sim$20 in the early Archean, and it takes more than 1 Gyr for μ^{142}_{Nd} to be reduced to approximately zero. If mantle mixing is responsible for this gradual decrease in μ^{142}_{Nd}, its long timescale may not be consistent with the operation of plate tectonics.

This interpretation of the ^{142}Nd evolution is, however, questionable on at least two accounts. First, inefficient mantle mixing by itself does not necessarily preclude the possibility of plate tectonics. Various kinds of geological evidence suggest that the tempo of plate tectonics was not faster in the past (Bradley, 2008; Herzberg et al., 2010; Padhi et al., 2012; Condie et al., 2015; Pehrsson et al., 2016; Korenaga et al., 2017), which could reduce the efficiency of mantle mixing

substantially (Korenaga, 2006). Second, and more important, the ^{142}Nd evolution can also be interpreted as the result of crustal recycling (Caro et al., 2006, 2017; Roth et al., 2014), as opposed to mantle mixing. Between these two possibilities, the interpretation with crustal recycling has the advantage of being able to be tested against crustal age data. In this study, therefore, we choose to pursue this alternative idea in a systematic manner. As shown later, the present-day distribution of crustal formation ages, as well as the current rate of sediment subduction, provides strong support to the interpretation based on crustal recycling. The coupled ^{143}Nd and ^{142}Nd evolution indicates the occurrence of intensive crustal generation and recycling throughout the early Earth, and we will discuss the implications of such crustal evolution for Hadean and Archean geodynamics.

2 Model Setup

We employ a box modeling approach to study the evolution of $\varepsilon_{\mathrm{Nd}}^{143}$ and μ_{Nd}^{142} in the continental crust and depleted mantle. The isotopes involved are the parent isotopes ^{147}Sm and ^{146}Sm, their radiogenic daughters ^{143}Nd and ^{142}Nd, and the non-radiogenic isotope ^{144}Nd. The initial composition of the mantle is equal to the composition of the bulk silicate Earth (BSE). The masses of the depleted mantle and the continental crust are given by $M_m(t)$ and $M_c(t)$, respectively. The rate of mass gained or lost by the depleted mantle is given by $\dot{M}_d(t)$ and $\dot{M}_u(t)$, respectively (overdot stands for time derivative). The net growth of the continental crust is given by $\dot{M}_c = \dot{M}_u - \dot{M}_d$. The total mass of the system is always conserved as $\dot{M}_c = -\dot{M}_m$. Continental crust growth and recycling are parameterized as

$$M_c(t) = \frac{M_c(t_p)}{1 - e^{-\kappa_g (t_p - t_s)}} \left(1 - e^{-\kappa_g (t - t_s)}\right), \tag{1}$$

and

$$\dot{M}_d(t) = R_s + \frac{R_p - R_s}{1 - e^{-\kappa_r (t_p - t_s)}} \left(1 - e^{-\kappa_r (t - t_s)}\right), \tag{2}$$

where t_s and t_p correspond to, respectively, the time when crustal growth and recycling started and the present-day (4.56 Gyr after the solar system initial). The terms R_s and R_p are the recycling rates at $t = t_s$ and $t = t_p$, respectively, and κ_g and κ_r are decay constants for crustal growth and recycling rate. Both $M_c(t)$ and $\dot{M}_d(t)$ are set to zero for $t < t_s$ and, the present-day value for the crustal mass $M_c(t_p)$ is set to 2.09×10^{22} kg. By varying t_s, κ_g, κ_r, R_s, and R_p, we can test a wide range of scenarios for crustal growth and recycling. Eqs. (1) and (2) can handle only monotonic variations, but they are sufficiently flexible to allow us to reproduce the first-order features of Nd isotope evolution.

Following DePaolo (1980), the mass balance equations for the parent (j), the daughter (i'), and the reference isotope (i) in the mantle are given by

$$\begin{aligned}
\dot{M}_m C_m^j + M_m \dot{C}_m^j &= \dot{M}_d C_c^j - \dot{M}_u D_j C_m^j - \lambda_j N_m^j, \\
\dot{M}_m C_m^{i'} + M_m \dot{C}_m^{i'} &= \dot{M}_d C_c^{i'} - \dot{M}_u D_i C_m^{i'} + \lambda_j N_m^j, \\
\dot{M}_m C_m^i + M_m \dot{C}_m^i &= \dot{M}_d C_c^i - \dot{M}_u D_i C_m^i,
\end{aligned} \tag{3}$$

where the subscripts m and c stand for mantle and crust, C are the concentrations of the different species, D are the crustal enrichment factors, λ is the decay constant, and N is the total number of atoms, with similar equations for the concentrations in the continental crust. The crustal enrichment factors control elemental partitioning upon the generation of new continental crust. The genesis of continental crust cannot be represented by single-stage mantle melting, and it is generally believed to involve multiple processes such as intracrustal differentiation, metasomatism, and crustal delamination. An enrichment factor should thus be regarded as an 'effective' parameter that quantifies the overall partitioning behavior resulting from such multiple processes.

Regarding the initial condition of μ_{Nd}^{142}, a deficit of $\sim$20 observed in chondritic meteorites with respect to the terrestrial standard has been suggested to require either a super-chondritic Earth or global BSE differentiation into an early depleted reservoir and an early enriched reservoir (Boyet and Carlson, 2005). Recently, however, this deficit has been shown to be the result of the Earth

having a larger component of the slow neutron-capture process (s-process) with respect to chondrites (Bouvier and Boyet, 2016; Burkhardt et al., 2016). Therefore, the initial conditions for the BSE are calculated through standard radioactive equations from the present-day isotope ratios for the CHUR and terrestrial standard (Jacobsen and Wasserburg, 1984; Boyet and Carlson, 2005; Bouvier et al., 2008; Marks et al., 2014; Sanborn et al., 2015): $(^{147}\mathrm{Sm}/^{144}\mathrm{Nd})_{t_0}^{\mathrm{CHUR}} = 0.201942$, $(^{143}\mathrm{Nd}/^{144}\mathrm{Nd})_{t_0}^{\mathrm{CHUR}} = 0.506687$, $(^{146}\mathrm{Sm}/^{144}\mathrm{Nd})_{t_0}^{\mathrm{CHUR}} = 0.000336$, and $(^{142}\mathrm{Nd}/^{144}\mathrm{Nd})_{t_0}^{\mathrm{std}} = 1.141511$, where t_0 denotes the solar system initial, and $(^{146}\mathrm{Sm}/^{144}\mathrm{Nd})_{t_0}^{\mathrm{CHUR}}$ is calculated from $(^{146}\mathrm{Sm}/^{144}\mathrm{Sm})_{t_0}^{\mathrm{CHUR}}$ and $(^{144}\mathrm{Sm}/^{144}\mathrm{Nd})_{t_p}^{\mathrm{CHUR}}$.

Our modeling strategy is to focus on the secular evolution of the *average* composition of the depleted component in the mantle, and we do not attempt to model isotopic variability in the mantle, for the following two reasons. First, it is difficult to reliably estimate the isotopic variability of source mantle for igneous rocks found in continental setting, because of various possibilities of crustal contamination. When judging whether a piece of continental rock is 'mantle-derived' or not, one of the common criteria is that its $\varepsilon_{\mathrm{Nd}}$ is sufficiently high, so published constraints on the Nd isotope evolution of the depleted mantle are already biased to the depleted end-member (commonly referred to as the depleted MORB-source mantle, where MORB stands for mid-ocean-ridge basalts (Zindler and Hart, 1986)). The problem is compounded for ancient rocks because metamorphic changes to Sm/Nd ratios make it difficult to accurately determine the initial Nd isotopic composition. Second, modeling isotopic variability involves more assumptions than modeling average compositions (Allegre and Lewin, 1995; Caro et al., 2006; Roth et al., 2014). The processes assumed for the source of variability in the dispersion modeling are unlikely to be exhaustive, and validating the assumptions made for mixing processes is difficult because the reality of mantle mixing is still largely unresolved, owing to the lack of accurate understanding of rock rheology (Manga, 1996; Korenaga and Karato, 2008; Jain et al., 2018).

Our model has ten free parameters in total: five parameters to describe crustal growth and recycling (t_s, κ_g, κ_r, R_s, and R_p), initial and final enrichment factors for Sm and Nd ($D_{\mathrm{Sm}}(t_s)$, $D_{\mathrm{Sm}}(t_p)$,

$D_{\mathrm{Nd}}(t_s)$, and $D_{\mathrm{Nd}}(t_p)$; enrichment factors vary linearly between the initial and final values), and the mass fraction of the depleted mantle with respect to the whole mantle, f_m. The *a priori* ranges for these parameters are set as follows: (4.37, 4.51) Ga for t_s, $(-1, 30)$ Gyr^{-1} for κ_g, $(-3, 3)$ Gyr^{-1} for κ_r, $(0, 5 \times 10^{22})$ kg Gyr^{-1} for R_s and R_p, (1, 50) for the enrichment factors, with the condition that $D_{\mathrm{Sm}} < D_{\mathrm{Nd}}$ all the times, and (0.1, 0.9) for f_m. The range of t_s corresponds to the oldest terrestrial zircon (Valley et al., 2014) and the separation of the silicate reservoirs due to the Moon-forming event (Barboni et al., 2017). The depleted mantle in our box model does not necessarily correspond to the shallow part of the convecting mantle; it is more of abstract nature, representing the fraction of the mantle that is chemically complementary to the continental crust, and it may be physically distributed throughout the mantle. The volume of this depleted component is time-independent as in the original formulation of DePaolo (1980), and unlike some of previous box modeling studies (e.g., McCulloch and Bennett, 1994), its interaction with the more primitive component is not considered; doing so would add at least one more free parameter, thereby increasing the nonuniqueness of box modeling. The rarity of the early Archean and Hadean rocks that exhibit positive Nd isotopic anomalies may indicate that the volume of the depleted mantle was considerably smaller in the early Earth, but such rarity may simply have resulted from the combined effects of crustal recycling and reworking over the Earth history. Our modeling strategy is to adopt something simple (the time-independent depleted mantle component) yet sufficiently flexible (our parameterization of crustal growth and recycling) and then validate our assumptions by comparing model predictions with independent constraints on crustal evolution.

3 Results

We conducted the Monte Carlo sampling of the aforementioned parameter space using the Mersenne Twister (Matsumoto and Nishimura, 1998) as a pseudo-random number generator, with the total number of iterations up to 4.5×10^7. The solutions were first screened by their ability to reproduce the crust and mantle concentrations of Sm and Nd at the present day: C_{Sm} between 2.7 and

154 5.1 ppm and $C_{\rm Nd}$ between 14 and 26 ppm for the crust, and $C_{\rm Sm}$ between 0.24 and 0.47 ppm and
155 $C_{\rm Nd}$ between 0.58 and 1.45 ppm for the depleted mantle (Korenaga, 2009). With this screening, the
156 number of the valid solutions was reduced to $\sim 8 \times 10^6$. These solutions were then further screened
157 using their deviations from the observed ^{143}Nd and ^{142}Nd evolution, as follows. We define the total
158 misfit, M, as

$$M = \log_{10} \left[\frac{(\sigma_\varepsilon - \min(\sigma_\varepsilon))^2}{\Delta_\varepsilon^2} + \frac{(\sigma_\mu - \min(\sigma_\mu))^2}{\Delta_\mu^2} \right], \tag{4}$$

159 where σ_ε is given by

$$\sigma_\varepsilon = \left\{ \sum_{k=1}^{n} \frac{1}{n} \left[\varepsilon_{\rm Nd}^{143}(t_k) - (\varepsilon_{\rm Nd}^{143})_k \right]^2, \right\}^{1/2} \tag{5}$$

160 with $\varepsilon_{\rm Nd}^{143}(t_k)$ denoting model prediction at $t = t_k$, and σ_μ is defined similarly with $\mu_{\rm Nd}^{142}$. A pair of
161 t_k and $(\varepsilon_{\rm Nd}^{143})_k$ or $(\mu_{\rm Nd}^{142})_k$ is called an anchor point, and we used six anchor points for σ_ε: (3.96,
162 2.5), (3.75, 1.97), (3.4, 2.88), (1.92, 3.95), (0.625, 7.75), and (0, 10), and five anchor points for σ_μ:
163 (3.80, 15), (3.4, 9), (2.66, 5), (1.48, 0), and (0, 0) (all ages are in Ga). These anchor points were
164 chosen to select the solutions that can mimic the gross behavior of Nd isotope evolution. Whereas
165 recent studies on Archean and Hadean terranes suggest that negative $\mu_{\rm Nd}^{142}$ anomalies may be more
166 common than the positive ones (e.g., O'Neil et al., 2012; Roth et al., 2014; Caro et al., 2017;
167 Morino et al., 2017), focusing on the positive side of the $\mu_{\rm Nd}^{142}$ anomalies is consistent with our
168 modeling strategy of the depleted mantle component. The term $\min(\sigma_{\varepsilon,\mu})$ denotes the minimum
169 value of $\sigma_{\varepsilon,\mu}$ among all solutions, and as the amplitude of $\mu_{\rm Nd}^{142}$ variation is about twice as large as
170 that of $\varepsilon_{\rm Nd}^{143}$ variation, we set $\Delta_\varepsilon = 1$ and $\Delta_\mu = 2$ to balance different isotope constraints. A solution
171 with the total misfit less than 0.5 appears to provide a reasonable fit to the observed Nd evolution,
172 and the number of such solutions is $\sim 2 \times 10^4$. The statistical representation of this successful
173 Monte Carlo ensemble is given in Figs. 1 and 2.

174 For crustal growth, κ_g is varied from -1 to 30 Gyr^{-1}, covering from linear crustal growth to
175 nearly instantaneous growth. For crustal recycling, R_s and R_p are varied from 0 to 5×10^{22} kg Gyr^{-1},
176 to model both increasing and decreasing trends, and κ_r is varied from -3 Gyr^{-1} to 3 Gyr^{-1} so that

the temporal evolution of recycling rate can be either concave upward or downward. Successful cases are, however, all characterized by rapid crustal growth ($\kappa_g > \sim 4$ Gyr^{-1}; Figs. 1c and 2a) and high recycling rate in the Hadean ($R_s \sim 2 \times 10^{22}$ kg Gyr^{-1}), with a gradual fourfold decrease over the Earth history (Fig. 1d). Rapid crustal growth is necessary to achieve the high $\mu^{142}_{\rm Nd}$ values at $\sim$4 Ga, and intensive crustal recycling must occur concurrently to reproduce its steady decrease over the Archean (Fig. 1b). The extent of crustal recycling should wane subsequently to match the overall $\varepsilon^{143}_{\rm Nd}$ evolution (Fig. 1a). Within the *a priori* range of the growth start time t_s (4.37 to 4.51 Ga), the successful solutions prefer the earlier onset of crustal genesis (Fig. 2e), and this is consistent with the suggestion that the Earth had a continental crust already at 4.4 Ga (Mojzsis et al., 2001; Wilde et al., 2001; Harrison et al., 2005). The crustal enrichment factors are only loosely constrained at $\sim$30-40 for Nd and $\sim$10-20 for Sm, and no major temporal change seems to be required for them (Fig. 2f,g). The mass fraction of the depleted mantle peaks at $\sim$0.3 (Fig. 2h), similar to what classical box modeling studies suggest (e.g., Jacobsen and Wasserburg, 1979), but its probability distribution is rather diffuse, with the 90 % confidence limit ranging from 0.23 to 0.62, reflecting the imprecise nature of geochemical mass balance (Allegre et al., 1983; Lyubetskaya and Korenaga, 2007). By the nature of our screening, model predictions for the present-day Sm and Nd concentrations in the crust and mantle are all within the acceptable ranges (Figs. 2i-l).

To better understand how crustal growth and recycling are constrained by the coupled ^{143}Nd and ^{142}Nd evolution, a few illustrative examples are given in Fig 3. The comparison of three different growth models, with the median recycling rate shown in Fig. 1d (dotted line), indicates that rapid crustal growth is constrained mostly by the ^{142}Nd evolution (Fig. 3, top row). Because ^{146}Sm was effectively extinct by the end of the Hadean, the mantle has to be substantially depleted in the early Hadean to explain the high $\mu^{142}_{\rm Nd}$ values in the early Archean (Fig. 3c). As the half-life of ^{147}Sm is much longer than the age of the Earth, on the other hand, the ^{143}Nd evolution is not very sensitive to the details of crustal growth (Fig. 3b). By contrast, the long-term ^{143}Nd evolution is sensitive to the temporal evolution of crustal recycling (Fig. 3, bottom row). Using the

median growth curve shown in Fig. 1c (dotted line), three kinds of crustal recycling are compared: a time-decaying recycling rate, and two constant recycling rates of 1.2×10^{22} kg Gyr^{-1} and 0.1×10^{22} kg Gyr^{-1} (Fig. 3d). The case with the low recycling rate results in a mantle that is simply too depleted, and neither ^{143}Nd nor ^{142}Nd evolution can be reproduced. The observed decrease in μ_{Nd}^{142} during the Archean demands substantial crustal recycling but is relatively insensitive to how recycling varies with time (Fig. 3f). It can be seen that the ^{143}Nd evolution is what dictates the reduced recycling rate in the post-Archean era (Fig. 3e). Modeling results suggest that the 90 % confidence limit for the present-day recycling rate is $0.1-1.2\times10^{22}$ kg Gyr^{-1} (Fig. 1d), which encompasses geological estimates for the present-day crustal recycling rate based on sediment subduction (2.5−3.2 km^3 yr^{-1} (Scholl and von Huene, 2007; Stern and Scholl, 2010), which is equivalent to $0.7-0.9\times10^{22}$ kg Gyr^{-1} with a crustal density of 2700 kg m^{-3}). It is notable that our box modeling was able to reproduce an acceptable present-day recycling rate without using such a constraint in the modeling.

Our preferred model of continental growth suggests that, by the end of the Hadean, the continental crust was volumetrically equivalent to the present day (Fig. 1c). It does not mean, however, that the Hadean crust should occupy much of the present-day continental crust because the recycling of crust into the mantle was also more efficient in the early Earth (Fig. 1d). This can be readily quantified by calculating the present-day distribution of crustal formation ages from the box modeling results as follows. First, we denote the mass distribution of crustal formation ages at some time t by $m(t,\tau)$, where τ is the formation age. This distribution and the continental mass are related as

$$\int_0^t m(t,\tau)d\tau = M_c(t). \tag{6}$$

In our box modeling, the continental crust is treated as a single uniform reservoir, so when the crust is recycled at the rate of $\dot{M}_d(t)$, all the crust is affected uniformly, independent of formation

ages. The temporal evolution of $m(t,\tau)$ with this age-independent recycling may be expressed as

$$\frac{\partial m(t,\tau)}{\partial t} = \dot{M}_u(t)\delta(t-\tau) - \frac{\dot{M}_d(t)}{M_c(t)}m(t,\tau), \tag{7}$$

where $\delta(t)$ is the Dirac delta function. The present-day distribution $m(t_p,\tau)$ can then be calculated by integrating the above differential equation, starting at $t = 0$. Finally, the present-day cumulative distribution of formation ages, $F(\tau)$, is calculated as

$$F(\tau) = \frac{1}{M_c(t_p)}\int_0^\tau m(t_p,\tau')d\tau'. \tag{8}$$

Note that the age-independent recycling here does not mean that recycled materials at any given time contain all formation ages equally. As seen in Eq. (7), the crust is recycled in proportion to $m(t,\tau)$; for example, if the crust with the formation age of 3 Ga is twice as abundant than that with the formation age of 4 Ga, such proportionality is directly reflected in recycled materials. Also, it is important to understand that $m(t,\tau)$ represents the distribution of 'original' crustal formation ages, so the 'apparent' ages of recycled materials can deviate to younger ages because of crustal reworking. Some authors argue against crustal recycling in the early Earth by noting that all $<$3.5 Ga terrigenous sediments in active margins and continental settings have Nd and Hf model ages younger than 3.5 Ga (e.g., Iizuka et al., 2017), but such observation does not preclude the recycling of $>$3.5 Ga materials because those model ages are likely to have been affected by crustal reworking (Korenaga, 2018).

The present-day distribution of crustal formation ages computed from our modeling results shows that only $\sim$10 % and $\sim$30 % of the present-day crust are originally formed during the Hadean and the Archean, respectively (Fig. 4). More important, the formation age distribution based on the Sm-Nd isotope systems is in remarkable agreement with that estimated from the global compilation of zircon age data (Korenaga, 2018). The convergence of these two entirely independent estimates, based on different geochemical data as well as different methods, is en-

couraging, suggesting that the modeling strategy based on crustal recycling allows us to probe correctly the origin of the observed Nd isotope evolution. As indicated in Fig. 4, the difference between the formation age distribution and the surface age distribution reflects the effect of crustal reworking, i.e., the remobilization of preexisting crust by partial melting or erosion and sedimentation. About 10 % of present crust having already existed in the Hadean may appear too high, given that the documented occurrence of pre-3.8 Ga rocks is rather rare on Earth. However, older rocks are subject to a greater likelihood of being affected by crustal reworking, and the most of the Hadean crust could have been sourced for younger crust (e.g., O'Neil and Carlson, 2017).

4 Discussion

Our modeling results are characterized by rapid crustal growth in the early Earth and gradually declining crustal recycling, both of which are qualitatively similar to the model of Armstrong (1981). In the Armstrong model, the continental crust does not achieve the present-day mass before $\sim$3.6 Ga, but this part of his model is largely speculative and not observationally constrained. The model of Campbell (2003) is based on the secular evolution of Nb/U of the mantle, the original data of which do not demand notable crustal growth since the early Archean, and the diminishing Hadean crustal mass in his model is based mostly on the scarcity of Hadean zircons, which can instead be explained by efficient crustal recycling as our modeling results indicate and also by crustal reworking (Korenaga, 2018). Some authors argue for subdued crustal recycling in the Hadean based on the preservation of Hadean precursor in Archean rocks (Caro et al., 2017), but such preservation by itself does not quantify the efficiency of crustal recycling. Even with the recycling rate several times greater than the present-day rate (Fig. 1d), a fraction of the crustal material originally produced in the Hadean can remain on the Earth's surface to the present (Fig. 4).

Crustal recycling in the early Earth is estimated as $\sim 2 \times 10^{22}$ kg Gyr^{-1} and can be as high as $\sim 4 \times 10^{22}$ kg Gyr^{-1} (Fig. 1d). Interestingly, the same level of recycling has also been suggested by the modeling of isotopic dispersion (Caro et al., 2006; Roth et al., 2014); with the crustal mass of

$\sim 2 \times 10^{22}$ kg, the crustal residence time of 0.5-0.75 Gyr suggested by these studies is equivalent to the recycling rate of 2.7-4$\times 10^{22}$ kg Gyr^{-1}, which is considerably higher than the present-day rate of recycling. As mentioned earlier, the validity of dispersion modeling is uncertain, but arriving at a similar conclusion with different modeling assumptions may attest to the robustness of the conclusion.

The ^{142}Nd evolution has commonly been interpreted to reflect early global differentiation followed by progressive remixing of an early differentiated reservoir, located at surface as continental crust or in the deep mantle (Caro et al., 2006; Bennett et al., 2007; Rizo et al., 2012; Debaille et al., 2013; Roth et al., 2014). In this study, we have focused on the possibility of the former, but other interpretations are also possible (e.g., Morino et al., 2017). Geophysical considerations are usually brought up to evaluate the strengths and weaknesses of different interpretations, but we must bear in mind that our understanding of subsolidus mantle convection is still not sufficiently mature to allow its reliable extrapolation to early Earth conditions. For example, it is almost always assumed that mantle mixing in the early Earth was efficient because the mantle was hotter. Even though the mantle was most likely hotter in the past because of the secular cooling of the Earth (Herzberg et al., 2010), a hotter mantle does not necessarily imply more vigorous convection (e.g., Solomatov, 1996; Korenaga, 2011); mantle viscosity depends not only on temperature but also on grain size and water content. How a putative magma ocean might have solidified suffers from even greater uncertainties. Instead of extracting the continental crust, the formation of Mg-perovskite cumulates in a crystallizing magma ocean can also create a high Sm/Nd reservoir (Corgne et al., 2005), but the lower mantle could have solidified fully by equilibrium crystallization (Solomatov, 2015), under which elemental fractionation would not occur.

Given the current state of science in geodynamics, we have so far avoided to intermingle geodynamical speculations with geochemical interpretations. Our strategy is to first focus on modeling the Nd isotope evolution in the framework of continental growth and recycling, and then discuss the geophysical implications of modeling results. Unlike other possible interpretations, our inter-

pretation of the Nd isotope evolution has an advantage of being supported quantitatively by two independent observations: (1) the present-day rate of sediment subduction, and (2) the present-day distribution of crust formation ages. Exploring its implications for early Earth geodynamics is thus of some merit. In doing so, it is important to recognize that to maintain zero net crustal growth after the Hadean (Fig. 1c) in the presence of intensive crustal recycling (Fig. 1d), the rate of new crustal generation has to match that of recycling. Therefore, even though the extremely rapid crustal growth in the early Hadean may in part reflect the solidification of the putative magma ocean, subsolidus mantle convection in the Archean must have been able to steadily produce the continental crust at the rate of $\sim 2 \times 10^{22}$ kg Gyr^{-1} and then destroy it at a similar rate (cf. the rate of oceanic crust production in present-day plate tectonics is $\sim 7 \times 10^{22}$ kg Gyr^{-1} (Crisp, 1984)). It is unclear whether such intensity of crustal evolution is compatible with stagnant lid convection or intermittent plate tectonics. A theoretical basis for intermittent plate tectonics in the early Earth has recently been shown to be questionable (Korenaga, 2017), and it would be more straightforward to explain our model of crustal evolution if plate tectonics was already operational in the early Earth (Hopkins et al., 2010).

In case of the continuous operation of plate tectonics throughout the Earth history, thermal evolution modeling suggests that average plate velocity in the past cannot be very different from the present-day value (Korenaga, 2011), and such thermal evolution is consistent with the cooling history of the upper mantle at least for the last 3.5 Gyr (Herzberg et al., 2010). Gradual decline in the rate of crustal generation may be explained by the secular cooling of the mantle, i.e., mantle melting was more extensive in the past, but the rate of crustal recycling has to decrease as well, which seems to be at odds with the relatively constant plate velocity through time. Its fourfold decrease over the Earth history (Fig. 1d) resembles the decay of internal heat generation (e.g., Turcotte and Schubert, 1982), but internal heat generation is not expected to manifest so directly in the tempo of tectonic processes, given our understanding of mantle convection in the Earth (Korenaga, 2016). Instead, the decline in crustal recycling may be explained by the greater preservation potential of

continental crust, which can be attained by the "cratonization" of continental crust (e.g., Cawood et al., 2013; Hawkesworth et al., 2017) or by the relative strengthening of continental mantle lithosphere owing to the hydration of convecting mantle (Korenaga, 2013). Even with the same tempo, the influence of plate tectonics on the surface environment could potentially be diverse because the physical and chemical state of the Earth's interior has steadily been changing with time. Our understanding of such interaction between plate tectonics and the surface environment is still largely undeveloped.

Acknowledgments

This material is based upon work supported in part by the U.S. National Aeronautics and Space Administration through the NASA Astrobiology Institute under Cooperative Agreement No. NNA15BB03A issued through the Science Mission Directorate and by the U.S. National Science Foundation under grant EAR-1753916. The authors thank Stephen Mojzsis and Richard Carlson for a number of constructive comments and suggestions, which helped to improve the accuracy and clarity of the manuscript.

References

Allegre, C. J., Hart, S. R., Minster, J.-F., 1983. Chemical structure and evolution of the mantle and continents determined by inversion of Nd and Sr isotopic data, II. numerical experiments and discussion. Earth Planet. Sci. Lett. 66, 191–213.

Allegre, C. J., Lewin, E., 1995. Isotopic systems and stirring times of the Earth's mantle. Earth Planet. Sci. Lett. 136, 629–646.

Armstrong, R. L., 1981. Radiogenic isotopes: the case for crustal recycling on a near-steady-state no-continental-growth Earth. Phil. Trans. R. Soc. Lond. A 301, 443–472.

346 Baadsgaard, H., Nutman, A. P., Bridgwater, D., 1986. Geochronology and isotopic variation of the early
347 Archaean Amitsoq gneisses of the Isukasia area, southern West Greenland. Geochim. Cosmochim.
348 Acta 50, 2173–2183.

349 Barboni, M., Boehnke, P., Keller, B., Kohl, I. E., Schoene, B., Young, E. D., McKeegan, K. D., 2017. Early
350 formation of the Moon 4.51 billion years ago. Sci. Adv. 3, e1602365.

351 Bennett, V. C., 2003. Compositional evolution of the mantle. In: Holland, H. D., Turekian, K. K. (Eds.),
352 Treatise on Geochemistry. Vol. 2. Elsevier, pp. 493–519.

353 Bennett, V. C., Brandon, A. D., Nutman, A. P., 2007. Coupled ^{142}Nd-^{143}Nd isotopic evidence for Hadean
354 mantle dynamics. Science 318, 1907–1910.

355 Bouvier, A., Boyet, M., 2016. Primitive Solar System materials and Earth share a common initial ^{142}Nd
356 abundance. Nature 537, 399–402.

357 Bouvier, A., Vervoort, J. D., Patchett, P. J., 2008. The Lu-Hf and Sm-Nd isotopic composition of CHUR:
358 Constraints from unequilibrated chondrites and implications for the bulk composition of terrestrial plan-
359 ets. Earth Planet. Sci. Lett. 273, 48–57.

360 Boyet, M., Carlson, R. W., 2005. ^{142}Nd evidence for early (>4.53 Ga) global differentiation of the silicate
361 Earth. Science 309, 576–581.

362 Bradley, D. C., 2008. Passive margins through earth history. Earth-Sci. Rev. 91, 1–26.

363 Burkhardt, C., Borg, L. E., Brennecka, G. A., Shollenberger, Q. R., Dauphas, N., Kleine, T., 2016. A
364 nucleosynthetic origin for the Earth's anomalous ^{142}Nd composition. Nature 537, 394–398.

365 Campbell, I. H., 2003. Constraints on continental growth models from Nb/U ratios in the 3.5 Ga Barberton
366 and other Archaean basalt-komatiite suites. Am. J. Sci. 303, 319–351.

367 Caro, G., Bourdon, B., Birck, J.-L., Moorbath, S., 2006. High-precision ^{142}Nd/^{144}Nd measurements in
368 terrestrial rocks: Constraints on the early differentiation of the Earth's mantle. Geochim. Cosmochim.
369 Acta 70, 164–191.

370 Caro, G., Morino, P., Mojzsis, S. J., Cates, N. L., Bleeker, W., 2017. Sluggish Hadean geodynamics: Ev-
371 idence from coupled ^{146,147}Sm-^{142,143}Nd systematics in Eoarchean supracrustal rocks of the Inukjuak
372 domain (québec). Earth Planet. Sci. Lett. 457, 23–37.

373 Cawood, P. A., Hawkesworth, C. J., Dhuime, B., 2013. The continental record and the generation of conti-
374 nental crust. GSA Bulletin 125, 14–32.

375 Condie, K., Pisarevsky, S., Korenaga, J., Gardoll, S., 2015. Is the rate of supercontinent assembly changing
376 with time? Precambrian Res. 259, 278–289.

377 Corgne, A., Liebske, C., Wood, B. J., Rubie, D. C., Frost, D. J., 2005. Silicate perovskite-melt partitioning
378 of trace elements and geochemical signature of a deep perovskite reservoir. Geochim. Cosmochim. Acta
379 69, 485–496.

380 Crisp, J. A., 1984. Rates of magma emplacement and volcanic output. J. Volcanol. Geotherm. Res. 20,
381 177–211.

382 Debaille, V., O'Neill, C., Brandon, A. D., Haenecour, P., Yin, Q.-Z., Mattielli, N., Treiman, A. H., 2013.
383 Stagnant-lid tectonics in early Earth revealed by ^{142}Nd variations in late Archean rocks. Earth Planet.
384 Sci. Lett. 373, 83–92.

385 DePaolo, D. J., 1980. Crustal growth and mantle evolution: inferences from models of element transport
386 and Nd and Sr isotopes. Geochim. Cosmochim. Acta 44, 1185–1196.

387 Goodwin, A. M., 1996. Principles of Precambrian Geology. Academic Press, London.

388 Harrison, T. M., Blichert-Toft, J., Müller, W., Albarede, F., Holden, P., Mojzsis, S. J., 2005. Heterogeneous
389 Hadean hafnium: Evidence of continental crust at 4.4 to 4.5 Ga. Science 310, 1947–1950.

390 Hawkesworth, C. J., Cawood, P. A., Dhuime, B., Kemp, A. I. S., 2017. Earth's continental lithosphere
391 through time. Annu. Rev. Earth. Sci. 45, 169–198.

392 Herzberg, C., Condie, K., Korenaga, J., 2010. Thermal evolution of the Earth and its petrological expression.
393 Earth Planet. Sci. Lett. 292, 79–88.

394 Holland, H. D., 1984. The Chemical Evolution of the Atmosphere and Oceans. Princeton University Press.

395 Hopkins, M. D., Harrison, T. M., Manning, C. E., 2010. Constraints on Hadean geodynamics from mineral
396 inclusions in >4 Ga zircons. Earth Planet. Sci. Lett. 298, 367–376.

397 Iizuka, T., Yamaguchi, T., Itano, K., Hibiya, Y., Suzuki, K., 2017. What Hf isotopes in zircon tell us about
398 crust-mantle evolution. Lithos 274-275, 304–327.

399 Jackson, M. G., Carlson, R. W., 2012. Homogeneous superchondritic $^{142}Nd/^{144}Nd$ in the mid-
400 ocean ridge basalt and ocean island basalt mantle. Geochem. Geophys. Geosys. 13, Q06011,
401 doi:10.1029/2012GC004114.

402 Jacobsen, S. B., Wasserburg, G. J., 1979. The mean age of mantle and crustal reservoirs. J. Geophys. Res.
403 84, 7411–7427.

404 Jacobsen, S. B., Wasserburg, G. J., 1984. Sm-Nd isotopic evolution of chondrites and achondrites, II. Earth
405 Planet. Sci. Lett. 67, 137–150.

406 Jain, C., Korenaga, J., Karato, S., 2018. On the grain-size sensitivity of olivine rheology. J. Geophys. Res.
407 Solid Earth 123, 674–688, https://doi.org/10.1002/2017JB014847.

408 Korenaga, J., 2006. Archean geodynamics and the thermal evolution of Earth. In: Benn, K., Mareschal, J.-C.,
409 Condie, K. (Eds.), Archean Geodynamics and Environments. American Geophysical Union, Washing-
410 ton, D.C., pp. 7–32.

411 Korenaga, J., 2009. A method to estimate the composition of the bulk silicate Earth in the presence of a
412 hidden geochemical reservoir. Geochim. Cosmochim. Acta 73, 6952–6964.

413 Korenaga, J., 2011. Thermal evolution with a hydrating mantle and the initiation of plate tectonics in the
414 early Earth. J. Geophys. Res. 116, B12403, doi:10.1029/2011JB008410.

415 Korenaga, J., 2013. Initiation and evolution of plate tectonics on Earth: Theories and observations. Annu.
416 Rev. Earth Planet. Sci. 41, 117–151.

417 Korenaga, J., 2016. Can mantle convection be self-regulated? Sci. Adv. 2, e1601168.

418 Korenaga, J., 2017. Pitfalls in modeling mantle convection with internal heating. J. Geophys. Res. Solid
419 Earth 122, 4064–4085, doi:10.1002/2016JB013850.

420 Korenaga, J., 2018. Estimating the formation age distribution of continental crust by unmixing zircon age
421 data. Earth Planet. Sci. Lett. 482, 388–395.

422 Korenaga, J., Karato, S., 2008. A new analysis of experimental data on olivine rheology. J. Geophys. Res.
423 113, B02403, doi:10.1029/2007JB005100.

424 Korenaga, J., Planavsky, N. J., Evans, D. A. D., 2017. Global water cycle and the coevolution of Earth's
425 interior and surface environment. Phil. Trans. R. Soc. A 375, 20150393, doi:10.1098/rsta.2015.0393.

426 Lyons, T. W., Reinhard, C. T., Planavsky, N. J., 2014. The rise of oxygen in Earth's early ocean and atmo-
427 sphere. Nature 506, 307–315.

428 Lyubetskaya, T., Korenaga, J., 2007. Chemical composition of Earth's primitive mantle and its variance, 2,
429 implications for global geodynamics. J. Geophys. Res. 112, B03212, doi:10.1029/2005JB004224.

430 Manga, M., 1996. Mixing of heterogeneities in the mantle: Effect of viscosity differences. Geophys. Res.
431 Lett. 23, 403–406.

432 Marks, N., Borg, L., Hutcheon, I., Jacobsen, B., Clayton, R., 2014. Samarium-neodymium chronology
433 and rubidium-strontium systematics of an Allende calcium-aluminum-rich inclusion with implications
434 for ^{146}Sm half-life. Earth Planet. Sci. Lett. 405, 15–24.

435 Matsumoto, M., Nishimura, T., 1998. Mersenne Twister: A 623-dimensionally equidistributed uniform
436 psedo-random number generator. ACM Trans. Model. Comp. Sim. 8, 3–30.

437 McCulloch, M. T., Bennett, V. C., 1994. Progressive growth of the Earth's continental crust and depleted
438 mantle: Geochemical constraints. Geochim. Cosmochim. Acta 58, 4717–4738.

439 Mojzsis, S. J., Harrison, T. M., Pidgeon, R. T., 2001. Oxygen-isotope evidence from ancient zircons for
440 liquid water at the Earth's surface 4,300 Myr ago. Nature 409, 178–181.

441 Moorbath, S., Whitehouse, M. J., Kamber, B. S., 1997. Extreme Nd-isotope heterogeneity in the early
442 Archaean - fact or fiction? case histories from northern Canada and West Greenland. Chem. Geol. 135,
443 213–231.

444 Morino, P., Caro, G., Reisberg, L., Schmacher, A., 2017. Chemical stratification in the post-magma ocean
445 Earth inferred from coupled ^{146,147}Sm-^{142,143}Nd systematics in ultramafic rocks of the Saglek block
446 (3.25-3.9 Ga; northern Labrador, Canada). Earth Planet. Sci. Lett. 463, 136–150.

447 Murphy, D. T., Brandon, A. D., Debaille, V., Burgess, R., Ballentine, C., 2010. In search of a hidden long-
448 term isolated sub-chondritic ^{142}Nd/^{144}Nd reservoir in the deep mantle: Implications for the Nd isotope
449 systematics of the Earth. Geochim. Cosmochim. Acta 74, 738–750.

450 O'Neil, J., Carlson, R. W., 2017. Building Archean cratons from Hadean mafic crust. Science 355, 1199–
451 1202.

452 O'Neil, J., Carlson, R. W., Paquette, J.-L., Francis, D., 2012. Formation age and metamorphic history of the
453 Nuvvuagittuq greenstone belt. Precambrian Res. 220-221, 23–44.

454 O'Neill, C., Debaille, V., 2014. The evolution of Hadean-Eoarchaean geodynamics. Earth Planet. Sci. Lett.
455 406, 49–58.

456 Padhi, C. M., Korenaga, J., Ozima, M., 2012. Thermal evolution of Earth with xenon degassing: A self-
457 consistent approach. Earth Planet. Sci. Lett. 341-344, 1–9.

458 Pehrsson, S. J., Eglington, B. M., Evans, D. A. D., Huston, D., Reddy, S. M., 2016. Metallogeny and its
459 link to orogenic style during the Nuna supercontinent cycle. In: Z.-X., L., Evans, D. A. D., Murphy,
460 J. B. (Eds.), Supercontinent Cycles Through Earth History. Geological Society of London, pp. 83–94,
461 doi:10.1144/SP424.5.

462 Puchtel, I. S., Touboul, M., Blichert-Toft, J., Walker, R. J., Bra, A. D., Nicklas, R. W., Kulikov, V. K., Sam-
463 sonov, A. V., 2016. Lithophile and siderophile element systematics of Earth's mantle at the Archean-
464 Proterozoic boundary: Evidence from 2.4 Ga komatiites. Geochim. Cosmochim. Acta 180, 227–255.

Rizo, H., Boyet, M., Blichert-Toft, J., O'Neil, J., Rosing, M. T., Paquette, J.-L., 2012. The elusive Hadean enriched reservoir revealed by ^{142}Nd deficits in Isua Archaean rocks. Nature 491, 96–100.

Roth, A. S. G., Bourdon, B., Mojzsis, S. J., Rudge, J. F., Guitreau, M., Blichert-Toft, J., 2014. Combined ^{147,146}Sm-^{143,142}Nd constraints on the longevity and residence time of early terrestrial crust. Geochem. Geophys. Geosys. 15, 2329–2345.

Sanborn, M. E., Carlson, R. W., Wadhawa, M., 2015. ^{147,146}Sm-^{143,142}Nd, ^{176}Lu-^{176}Hf, and ^{87}Rb-^{87}Sr systematics in the angrites: Implications for chronology and processes on the angrite parent body. Geochim. Cosmochim. Acta 171, 80–99.

Scholl, D. W., von Huene, R., 2007. Crustal recycling at modern subduction zones applied to the past—issues of growth and preservation of continental basement, mantle geochemistry and supercontinent reconstruction. Geol. Soc. Am. Spec. Paper 200, 9–32.

Sleep, N. H., Zahnle, K. J., Lupu, R. E., 2014. Terrestrial aftermath of the Moon-forming impact. Phil. Trans. R. Soc. A 372, 20130172, doi:10.1098/rsta.2013.0172.

Solomatov, V., 2015. Magma oceans and primordial mantle differentiation. In: Treatise on Geophysics, 2nd ed. Vol. 9. Elsevier, pp. 81–104.

Solomatov, V. S., 1996. Can hotter mantle have a larger viscosity? Geophys. Res. Lett. 23, 937–940.

Stern, R. J., Scholl, D. W., 2010. Yin and yang of continental crust creation and destruction by plate tectonic processes. Int. Geol. Rev. 52, 1–31.

Turcotte, D. L., Schubert, G., 1982. Geodynamics: Applications of Continuum Physics to Geological Problems. John Wiley, New York.

Valley, J. W., Cavosie, A. J., Ushikubo, T., Reinhard, D. A., Lawrence, D. F., Larson, D. J., Clifton, P. H., Kelly, T. F., Wilde, S. A., Moser, D. E., Spicuzza, M. J., 2014. Hadean age for a post-magma-ocean zircon confirmed by atom-probe tomography. Nature Geosci. 7, 219–223.

Vervoort, J. D., Blichert-Toft, J., 1999. Evolution of the depleted mantle: Hf isotope evidence from juvenile rocks through time. Geochim. Cosmochim. Acta 63, 533–556.

490 Wilde, S. A., Valley, J. W., Peck, W. H., Graham, C. M., 2001. Evidence from detrital zircons for the
491 existence of continental crust and oceans on the Earth 4.4 Gyr ago. Nature 409, 175–178.

492 Zindler, A., Hart, S., 1986. Chemical geodynamics. Annu. Rev. Earth Planet. Sci. 14, 493–571.

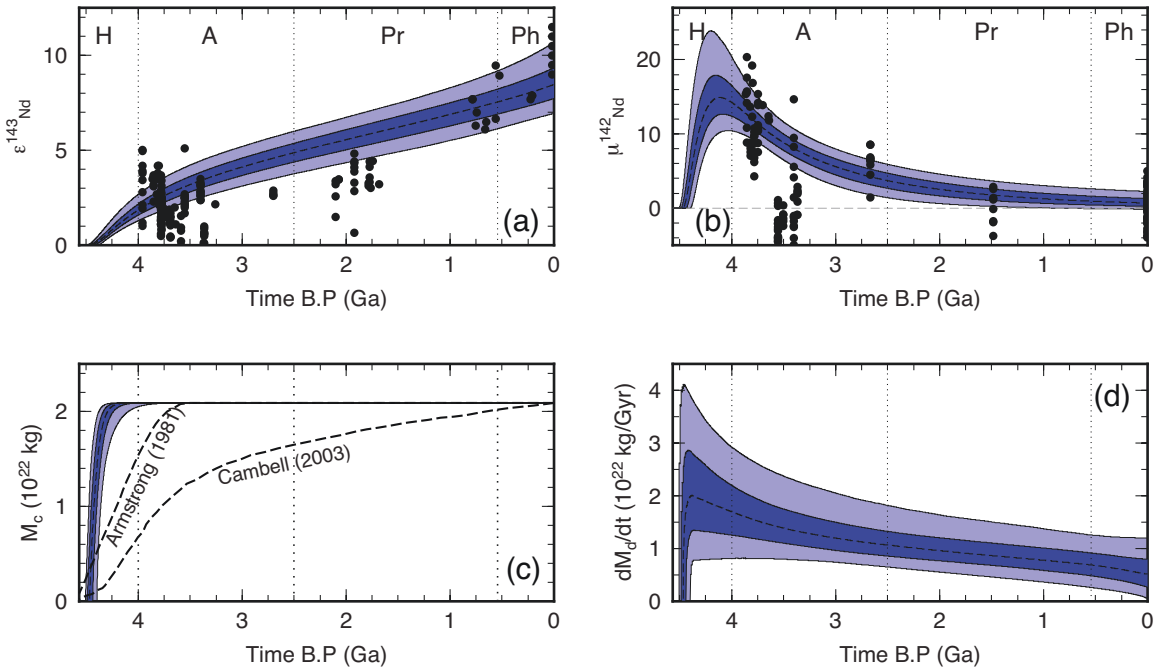

Figure 1: (a) ^{143}Nd and (b) ^{142}Nd evolution of the depleted mantle based on published data (Baadsgaard et al., 1986; Moorbath et al., 1997; Vervoort and Blichert-Toft, 1999; Caro et al., 2006; Bennett et al., 2007; Murphy et al., 2010; Rizo et al., 2012; Jackson and Carlson, 2012; Debaille et al., 2013; Roth et al., 2014; Puchtel et al., 2016; Caro et al., 2017; Morino et al., 2017) as a function of time before present, from $t = 4.567$ Ga (solar system initial) to $t = 0$ (present). $\varepsilon^{143}_{\mathrm{Nd}}(t)$ is defined as $[(^{143}\mathrm{Nd}/^{144}\mathrm{Nd})_t/(^{143}\mathrm{Nd}/^{144}\mathrm{Nd})^{\mathrm{CHUR}}_t - 1] \times 10^4$, and $\mu^{142}_{\mathrm{Nd}}(t)$ as $[(^{142}\mathrm{Nd}/^{144}\mathrm{Nd})_t/(^{142}\mathrm{Nd}/^{144}\mathrm{Nd})^{\mathrm{std}}_t - 1] \times 10^6$, where CHUR and std stand for the chondritic uniform reservoir and the terrestrial standard reference, respectively. Also shown are the results of box modeling corresponding to (c) crustal growth and (d) crustal recycling rate. Dark blue region denotes the inter-quartile range, representing the mid 50 % of all successful solutions, whereas light blue region covers from the 5th to 95th percentile. Dotted line represents the median. Vertical dotted lines divide the Earth history into the Hadean (H), the Archean (A), the Proterozoic (Pr) and the Phanerozoic (Ph). Previous models of net continental growth (Armstrong, 1981; Campbell, 2003) are also shown in (c) for comparison.

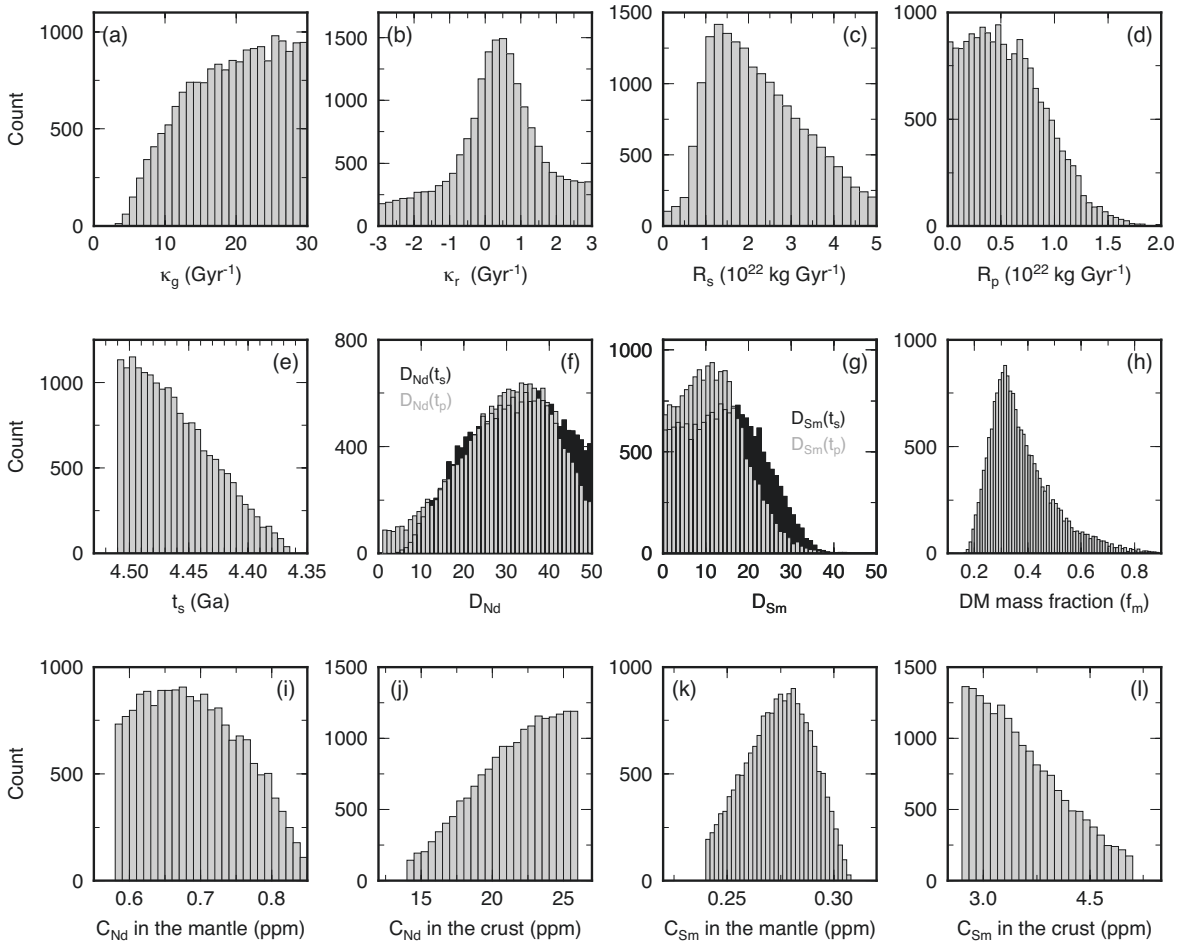

Figure 2: The a posteriori distributions of input model parameters and some model variables, based on $\sim 2 \times 10^4$ successful Monte Carlo solutions. (a) Decay constant for continental growth, (b) decay constant for crustal recycling, (c) initial recycling rate, (d) present-day recycling rate, (e) onset time for crustal generation and recycling, (f) initial (black) and present-day (gray) crustal enrichment factors for Nd , (g) crustal enrichment factors for Sm, (h) mass fraction of the depleted mantle, (i) Nd concentration in the depleted mantle, (j) Nd concentration in the continental crust, (k) Sm concentration in the depleted mantle, and (l) Sm concentration in the continental crust. The concentrations in (i)-(l) are all at the present day.

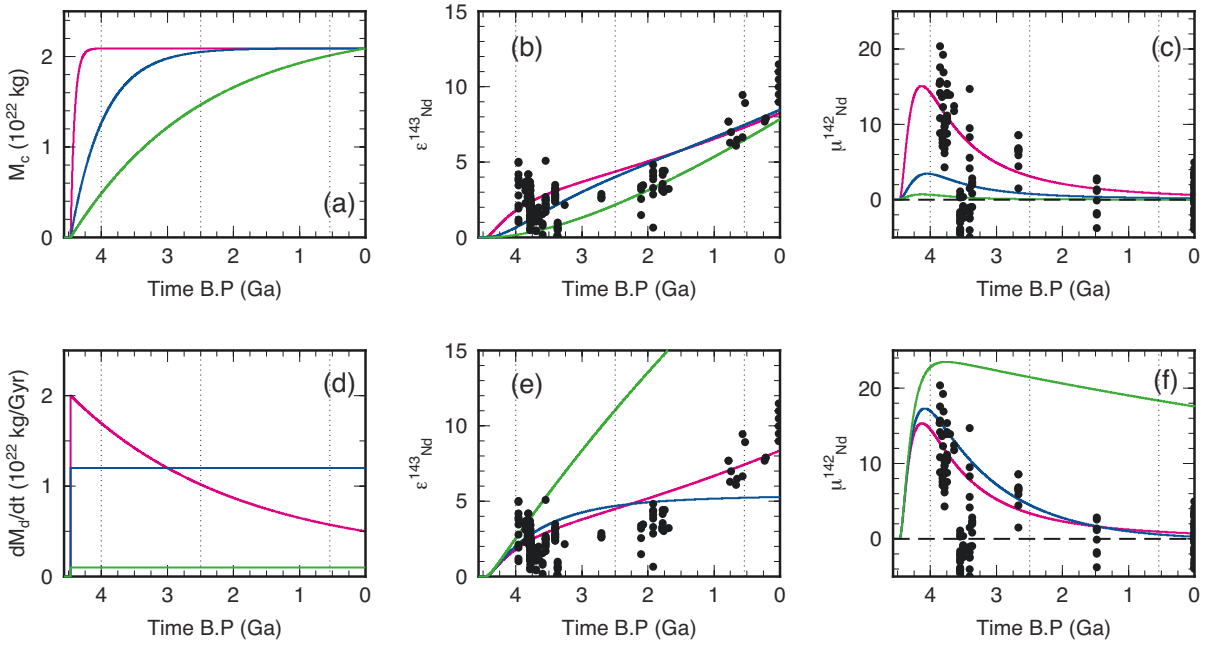

Figure 3: Top row: effect of crustal growth on the Nd isotope evolution. (a) Crustal growth functions using κ_g =0.5 (green), 2.0 (blue), and 17 (red) (b) Corresponding evolution of $\varepsilon^{143}_{\mathrm{Nd}}$, with the the median solution for the recycling rate (Fig. 1d). (c) Same as (b), but for μ^{142}_{Nd}. Bottom row: effect of crustal recycling. (d) Recycling rate functions using $R_s = 2.0 \times 10^{22}$ kg Gyr^{-1}, $R_p = 0.5 \times 10^{22}$ kg Gyr^{-1}, and $\kappa_r = 0.5$ (red), $R_s = R_p = 1.2 \times 10^{22}$ kg Gyr^{-1} and $\kappa_r = 0$ (blue), and $R_s = R_p = 0.10 \times 10^{22}$ kg Gyr^{-1} and $\kappa_r = 0$ (green). (e) Corresponding evolution of $\varepsilon^{143}_{\mathrm{Nd}}$, with the the median solution for crustal growth (Fig. 1c) (f) Same as (e), but for μ^{142}_{Nd}. All models share the following parameters: t_s=4.51 Ga, $D_{\mathrm{Nd}}(t_s)$=35, $D_{\mathrm{Nd}}(t_p)$=45, $D_{\mathrm{Sm}}(t_s)$=20, $D_{\mathrm{Sm}}(t_s)$=25, and f_m=0.35.

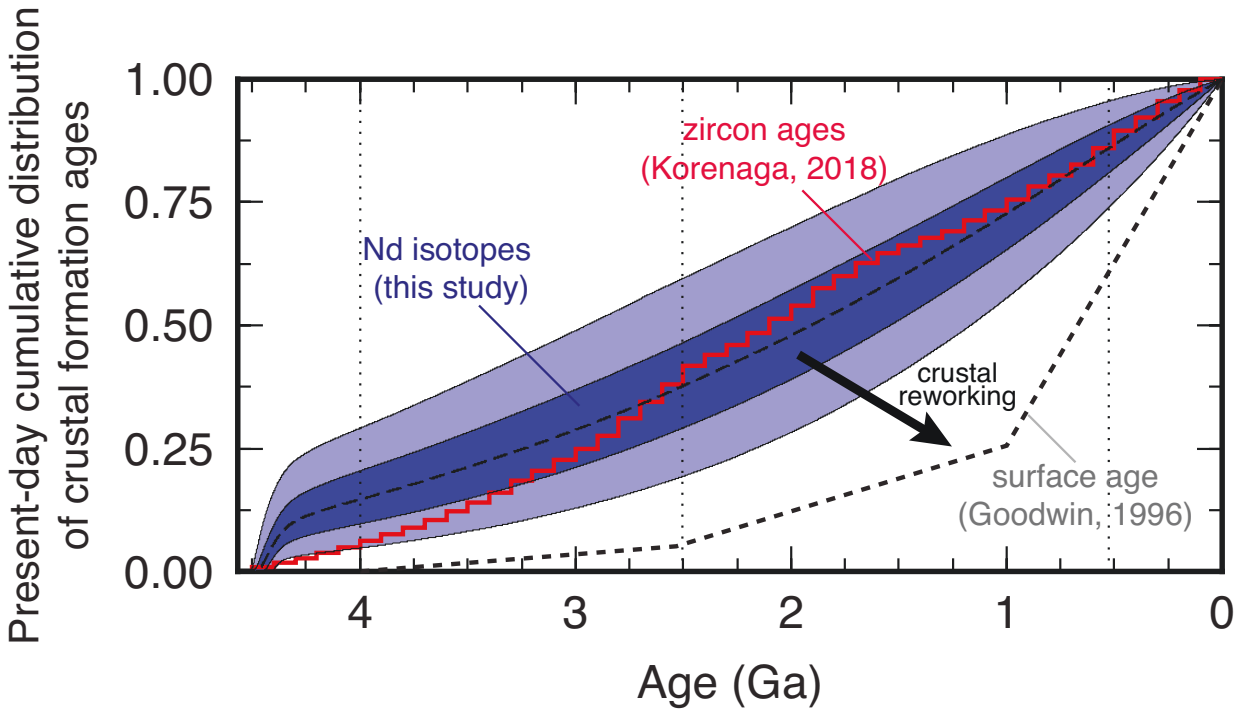

Figure 4: Present-day cumulative distribution of crustal formation age, as computed from crustal growth (Fig. 1c) and crustal recycling (Fig. 1d). The cumulative distribution is normalized by the present-day continental mass. The meaning of blue shadings are the same as in Fig. 1. An estimate based on the global compilation of zircon age data (Korenaga, 2018) (red) as well as the present-day surface age distribution (gray dotted) (Goodwin, 1996) are also shown for comparison. Difference between the distributions of formation ages and surface ages signifies the effect of crustal reworking.